Magnetic-field-enhanced transient and stationary drift currents of oscillating Bloch electrons in superlattices and limits of average-particle description in relation to Monte Carlo simulations

N. V. Demarina,[1] E. Mohler,[2] A. Lisauskas,[2] and H. G. Roskos[2]
[1]*Radiophysics Faculty, Nizhny Novgorod State University, 603950 Nizhny Novgorod, Russia*
[2]*Physikalisches Institut, Johann Wolfgang Goethe-Universität, D-60438 Frankfurt am Main, Germany*
(Received 24 June 2008; revised manuscript received 29 October 2009; published 7 December 2009)

We theoretically investigate transient and stationary drift currents of Bloch electrons in semiconductor superlattices subjected to an electric field along the growth axis and a magnetic field tilted with respect to the electric field. The magnetic-field-induced nonlinear coupling between the Bloch oscillations along the axis and in-plane cyclotron oscillations leads to a resonant phase-sensitive self-rectification of the oscillating currents. Both the transient motion of the particles after pulse excitation and the motion in the stationary state show this phenomenon. The effects have already been demonstrated experimentally but were discussed on the basis of different concepts. Here, we treat the transient and the stationary effect on equal footing using the model of the coupled oscillators. The relaxation and dephasing of the oscillations are explored with a Monte Carlo method and compared with results of models which use average-particle variables. It is found that average-particle-type models are not adequate to describe the resonance and relaxation effects of the ensemble satisfactorily. In the long-time limit and for strong coupling, they lead to some artifacts such as self-sustained oscillations or hysteresis effects, which do not exist in the Monte Carlo approach. The average-particle description is a qualitative approximation for weak coupling and if elastic scattering dominates. The shapes of the resonance curves in the Monte Carlo simulation sensitively depend on the details of the scattering mechanisms and allow us to identify their relative importance.

DOI: 10.1103/PhysRevB.80.245307 PACS number(s): 73.21.Cd, 73.23.−b, 42.60.Rn, 02.70.Uu

I. INTRODUCTION

The dynamics of electrons in semiconductor superlattices (SL) exposed to an electric field along the growth axis shows some peculiarities which are all based on the possibility of a SL electron to reach the boundary of the mini-Brillouin zone without scattering and to undergo a Bragg reflection there. Among the various effects connected with Bragg reflections are a current-voltage characteristics with negative differential conductivity,[1–7] transient Bloch oscillations of coherently excited electron bunches,[8–12] Bloch gain,[13–24] frequency mixing, and harmonic generation.[25–28]

Recently, the influence of an additional magnetic field tilted with respect to the electric field has been investigated in theory and experiment.[29–33] In the combined fields, an electron performs both Bloch oscillations along the SL axis and in-plane cyclotron oscillations. In addition, the Bloch oscillator (BO) and the cyclotron oscillator (CO) are nonlinearly coupled by the magnetic field, with the result that a resonantly enhanced self-induced dc of the BO flows during the transient as well as in the stationary state.

Both effects have been presented in quite different context. The transient effect[30] bears some analogies to the Fiske effect which is observed in Josephson junctions enclosed in a microwave cavity.[34] The enhancement of the stationary current has been related to chaotic dynamics of the electron motion in the nonlinear system,[31,33] where both the undamped motion[31] and the influence of linear damping of the cyclotron motion have been investigated. The purpose of the present paper is to treat the transient and the stationary effects on a common basis which consistently uses the picture of the coupled oscillators and gives some insight by drawing from results typical of electronic circuits. Furthermore, the relaxation of the oscillations are explored with Monte Carlo (MC) methods and are compared with results of models which use average-particle variables. Because of drastic discrepancies between the predictions of the different models, the problem is a touchstone for the theoretical methods generally used to treat nonlinear transport in SL.

II. THEORETICAL APPROACH

The essential features of the resonant enhancement of the dc can be elaborated by a semiclassical description of the oscillating electrons.[35] The miniband energy dispersion of Bloch electrons in the SL with spacing d and growth axis along the x direction is modeled as $E(\vec{k})=E_x(k_x)+E_\perp(k_y,k_z)$ with $E_x(k_x)=\hbar^2[1-\cos(k_x d)]/m_{xx}^0 d^2$ and $E_\perp(k_y,k_z)=\hbar^2(k_y^2+k_z^2)/2m_{yy}$, where m_{xx}^0 is the bottom effective mass of the miniband and m_{yy} the in-plane mass. In the following, we assume the carrier density to be sufficiently low so that field-screening and plasma effects[30,36] can be neglected. In the single-particle picture, the semiclassical equations of motion $\vec{V}=(1/\hbar)\partial E/\partial\vec{k}$ and $\hbar d\vec{k}/dt=e\vec{F}+e(\vec{V}\times\vec{B})$ for velocity $\vec{V}$ and momentum $\hbar\vec{k}$ of a wave packet in an electric field $\vec{F}$ and a magnetic field $\vec{B}$, then result in the following set of equations (assuming $\vec{F}$ to be parallel to the x axis and $\vec{B}$ to lie in the xz plane with tilt angle Θ against the x axis):

$$\dot{\phi}_x = \omega_B + \omega_{cz}\sqrt{A}v_y, \tag{1}$$

$$\dot{v}_y = \omega_{cx}v_z - \omega_{cz}\sin(\phi_x)/\sqrt{A}, \tag{2}$$

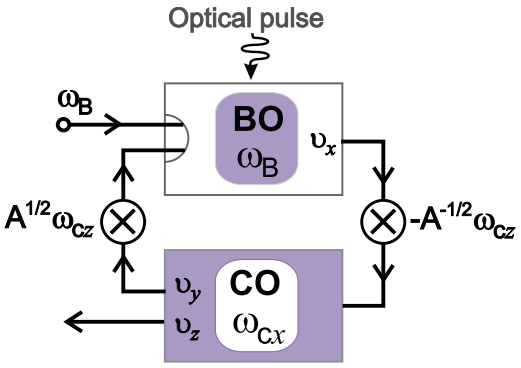

FIG. 1. (Color online) Schematic of coupled Bloch oscillator (BO) and in-plane cyclotron oscillator (CO) forming a feedback loop.

$$\dot{v}_z = -\omega_{cx} v_y. \tag{3}$$

The lowercase letters v denote scaled variables with V normalized to the maximum velocity $V_{max}=\hbar/m_{xx}^0 d$ along the x axis. The quantity $\phi_x=k_x d$ is the phase of the motion along the x direction, the corresponding velocity is given by $v_x=\sin(\phi_x)$. $A=m_{yy}/m_{xx}^0$ is the mass ratio. An equivalent set of equations was previously employed in Ref. 31 and partly in Ref. 33 for the description of the motion of Bloch-oscillating electrons in a magnetic field.

Equation (1) describes the BO with unperturbed frequency $\omega_B=eF_x d/\hbar$, and Eqs. (2) and (3) refer to the CO with frequency $\omega_{cx}=eB\cos(\Theta)/m_{yy}$. The coupling strength between the BO and the CO mediated by B_z is described by the frequency $\omega_{cz}=eB\sin(\Theta)/\sqrt{m_{xx}^0 m_{yy}}$. Note that the CO is amplitude driven by the BO whereas the BO is frequency modulated by the CO. The latter (parametric) mechanism is the reason for the nonlinear behavior of the coupled modes.

In Fig. 1, the coupling of the two oscillators by the set of differential equations is visualized in a flow diagram. The current oscillations of the BO (expressed by v_x) are driven by F_x, the x component of the electric field, which enters into the equations via the Bloch frequency ω_B. The coupling between the BO and the CO (in terms of the quantities v_x and v_y) via ω_{cz} is indicated by the circles. The diagram shows that the coupled oscillators form a closed feedback loop reminiscent of an electronic circuit consisting of a resonator (CO) and an active, voltage-controlled oscillator (BO). The circuit loosely resembles a phase-locked loop which is also known to display a great variety of nonlinear phenomena.

The rise of an additional resonant dc of the BO can be visualized as follows: starting from rest, the constant electric field F_x causes the BO to perform oscillations at the frequency ω_B which are then transferred to the CO. The rate of transfer, which depends on the coupling strength, is most effective if the frequencies of both oscillators are at resonance. From the CO, the oscillations are echoed back into the BO where they are mixed with the still-existing oscillations of the BO via frequency modulation. The modulation prolongs one half cycle of the BO and shortens the other, thus disturbing the balance of the current. The mixing (down conversion) therefore results in a dc of the BO whose strength and sign depend on the magnitude and on the relative phases of the BO and CO oscillations. The effect can also be viewed as a kind of phase-sensitive self-rectification where, in analogy to a lock-in amplifier, the CO oscillation represents the signal and the BO oscillation the reference signal.

At first sight, one expects the self-induced dc to vanish rapidly because both oscillations should lose their coherence by scattering. For example, if the phase of the BO mode changes by scattering of the electron wave packet, the phases of the oscillations will no longer be synchronous, and a dc of a different sign may arise by the mixing. Note, however, that damping of the motion due to inelastic scattering reduces the velocity amplitude of the CO oscillation and brings the phase of the BO back to near zero. Thus, although the amplitude of the BO oscillation of a single particle driven by the electric field remains constant, the reduced amplitude of the CO oscillation will already weaken the "wrong" nonlinear current. On the other hand, the disturbed BO immediately produces a new response of the CO such that the *relative* phase of the two oscillations and their amplitudes are recovered. The direction of the self-induced current is maintained. As a consequence, each particle in an ensemble produces a dc with the same sign, although the velocities of different particles may be completely uncorrelated. It is the correlation of the x and the y motions belonging to a specific particle which is responsible for the self-rectification effect.

In a stationary state, the component of the additional current along the electric field turns out to flow along the same direction as an already existing drift current, thus increasing the electrical power supplied by the field. For both currents to exist, a dissipation mechanism therefore is necessary in dynamic equilibrium.

To quantify these considerations, we solve the equations of motion numerically, assuming different models to describe scattering and relaxation. In all our simulations, a particle bunch is launched at $t=0$ at the bottom of the miniband (e.g., by optical-pulse excitation) and the transient currents as well as the stationary currents are calculated assuming temperature $T=0$ if not stated otherwise.

In the following, we first utilize simplified descriptions for scattering and relaxation which allows us to discuss extreme cases and hereby highlight the central features to be discussed in this paper. To explore limits we partly use values of coupling strength and scattering rates which might not be realistic and will even touch the validity of the oscillator picture as a visualization of the equations of motion. We then turn to state-of-the-art Monte Carlo simulations both to show that these features survive under realistic conditions and to investigate how they are modified.

III. AVERAGE-PARTICLE AND SIMPLIFIED MONTE CARLO MODELS

In a first step, we modify Eq. (1) by introducing velocity $v_x=\sin(\phi_x)$ and energy $\epsilon_x=[1-\cos(\phi_x)]$ as variables (ϵ_x equals E_x normalized to $\Delta/2$, where $\Delta=2\hbar^2/m_{xx}^0 d^2$ is the miniband width). One then has $\dot{v}_x=(\omega_B+\omega_{cz}\sqrt{A}v_y)(1-\epsilon_x)$ and $\dot{\epsilon}_x=(\omega_B+\omega_{cz}\sqrt{A}v_y)v_x$ instead of Eq. (1). Following the

common procedure,[37] we then substitute the single-particle variables $v_i(t)$, $i=x,y,z$, and $\epsilon_x(t)$ by average-particle (AP) variables $\langle v_i(t)\rangle$ and $\langle \epsilon_x(t)\rangle$, where $\langle\cdots\rangle$ denotes the time-dependent ensemble average. The averages of the single-particle product terms are substituted (factorized) by a product of AP variables.[39,41] Scattering is treated by adding phenomenological dissipative relaxation terms $-\Gamma\langle v_i(t)\rangle$, and $-\Gamma\langle \epsilon_x(t)\rangle$ on the right side of the corresponding differential equations which then read

$$\langle \dot{v}_x\rangle = (\omega_B + \omega_{cz}\sqrt{A}\langle v_y\rangle)(1-\langle \epsilon_x\rangle) - \Gamma\langle v_x\rangle, \tag{4}$$

$$\langle \dot{\epsilon}_x\rangle = (\omega_B + \omega_{cz}\sqrt{A}\langle v_y\rangle)\langle v_x\rangle - \Gamma\langle \epsilon_x\rangle, \tag{5}$$

$$\langle \dot{v}_y\rangle = \omega_{cx}\langle v_z\rangle - \omega_{cz}\langle v_x\rangle/\sqrt{A} - \Gamma\langle v_y\rangle, \tag{6}$$

$$\langle \dot{v}_z\rangle = -\omega_{cx}\langle v_y\rangle - \Gamma\langle v_z\rangle. \tag{7}$$

These approximations and the resulting balance equations have frequently been used in the literature.[38–41] In extension of the AP-type model of Ref. 33, where phenomenological damping of only the cyclotron motion was considered, the introduction of $\langle \epsilon_x\rangle$ and $\langle v_x\rangle$ as (now independent) variables allows to treat also direct damping and dephasing of the Bloch oscillations. As a consequence and in contrast to the model of Ref. 33 which is based on only three equations our four-dimensional (4D) AP model accurately describes important physical phenomena such as the drift current in the electric field due to inelastic scattering and the decay of Bloch oscillations of an electron ensemble optically excited in a SL. In the picture of the coupled oscillators, the active voltage-controlled BO is substituted by an oscillator with relaxation and drift current but with internal Bloch gain.[13]

In a second class of models, we solve the equations of motion without damping terms [i.e., by using Eqs. (1)–(3)] and treat relaxation and damping by the MC method. The free motion of a particle is interrupted by statistical scattering events which lead to a sudden change in its trajectory. We here apply a very simple type of scattering to calculate both the transient and the stationary currents. It is assumed that a particle experiences scattering with a probability independent of time and of the state of motion. We consider heuristically inelastic and elastic scatterings in simplified forms, with scattering rates Γ_{in} and Γ_{el} (corresponding overall scattering rate: $\Gamma_{in}+\Gamma_{el}$). In this picture, a particle shall lose all its energy in an inelastic collision and be reset to rest at the bottom of the miniband. Elastic scattering is treated such that the selection of the final state occurs with equal probability for the x component of the wave vector. The allowed final in-plane components are given statistically isotropic directions. For integration of the equation of motion we employ the classical fourth-order Runge-Kutta method[43] well known for its stability which is important for the simulation of the electron motion exhibiting chaotic trajectories. Averaging over an ensemble of 7×10^4 particles, we determine the time-dependent mean-velocity components $\langle v_i(t)\rangle$.

For the case of the MC model, we first assume that a particle ensemble is exposed to inelastic scattering only, i.e., $\Gamma_{in}=\Gamma$ and $\Gamma_{el}=0$. In this case, the continuous and the stochastic damping introduced in the two models are directly related to each other, allowing for a fair comparison of the results. Also, no random numbers are needed to calculate the ensemble average of the velocities since it is possible to express the average by an integral over the free (ballistic) motion. One obtains within this variant of the MC model for the velocity v_x,

$$\langle v_x(t)\rangle = e^{-\Gamma t}v_x^{free}(t) + \Gamma\int_0^t e^{-\Gamma t'}v_x^{free}(t')dt', \tag{8}$$

where $v_x^{free}(t)$ is the velocity of free motion starting at $t=0$ from rest ($\phi_x=0$, $v_y=v_z=0$). Corresponding equations are valid for $\langle v_y\rangle$ and $\langle v_z\rangle$.

The mean velocity consists of two terms. The first contribution in Eq. (8) originates from the particles which move without scattering until time t (the exponential factor $e^{-\Gamma t}$ describes the probability that the duration of scattering-free motion is larger than t). The second term in Eq. (8) is due to those particles which have been scattered (reset) at least once until t, and is derived as follows. Assuming that the last scattering of an electron occurred at time t' with probability $\Gamma dt'$, and again using the probability of scattering-free motion until at least t, one obtains, after integration over t' in the interval $[0,t]$, the velocity contribution $\Gamma\int_0^t e^{-\Gamma(t-t')}v_x^{free}(t-t')dt'$ which is just the second term of Eq. (8). For $t\to\infty$ the mean velocity $\langle v_x(t)\rangle$ approaches the familiar form of the kinetic equation $v_d=\Gamma\int_0^\infty v(t)\exp(-\Gamma t)dt$ for the stationary drift velocity.[31,42]

The coupled oscillators driven by the electric field show a great variety of responses which particularly for the AP model sensitively depend on the initial conditions, on the strength of the electric and magnetic fields, and on the parameters such as tilt angle, damping frequency, and mass ratio. For weak coupling and medium damping, the transients normally tend to stationary and stable solutions where the velocities and the energy for $t\to\infty$ relax to constant values $\langle v_i(\infty)\rangle$, $i=x,y,z$, and $\langle \epsilon_x(\infty)\rangle$. For increased coupling strength and reduced damping, the transients in the AP model generally tend to either limit cycles or erratic motion.

To illustrate the wealth of responses, Fig. 2 displays Fourier spectra $|v_x(\omega)|$ (coded by color and brightness) of the AP velocity $\langle v_x(t)\rangle$ during the transient as a function of Fourier frequency ω (vertical axis) and CO frequency ω_{cx} (horizontal axis), both normalized to ω_B. The two panels refer to different parameter sets of Θ, A, and Γ. The left panel shows spectra where relaxation and limit cycles dominate, the right panel with its noisy spectra shows signatures of irregular motion. In both panels, the traces of the various frequency combinations produced by mixing of ω_B and ω_{cx} and their harmonics through the nonlinearities of the BO can be nicely seen. The points where the traces meet at $\omega=0$ mark the characteristic resonance conditions which result in a dc by down conversion. Prominent responses are expected if the condition $\omega_{cx}/\omega_B=r$ is fulfilled, where r is a rational number.

We now compare the results of the AP and the MC models, first for parameter sets where the transient oscillations starting from zero converge to constant-current solutions.

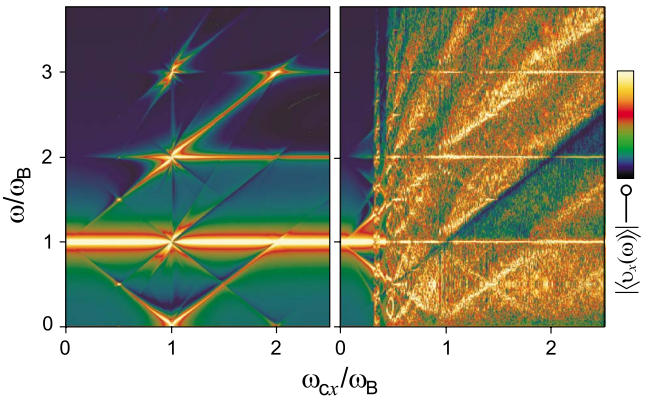

FIG. 2. (Color online) Map of the Fourier transform $|\langle v_x(\omega)\rangle|$ of the velocity $\langle v_x(t)\rangle$ for $0 \le \omega_B t \le 1000$ (coded as $\log\{1+1000|\langle v_x(\omega)\rangle|\}$ by pixel color and brightness) as a function of cyclotron frequency ω_{cx}/ω_B (horizontal scales) and Fourier frequency ω/ω_B (vertical scales), calculated with the AP model for $A=0.6$, $\Gamma=0.005\omega_B$, $\Theta=30°$ (left panel), and $\Theta=60°$ (right panel).

Figure 3 displays the mean velocity $\langle v_x(t)\rangle$ of the BO (the quantity which can be measured most directly through the electrical current along the SL axis), calculated with the two models for resonance ($\omega_{cx}=\omega_B$) and only inelastic scattering. The coupling strength is varied from zero coupling ($\Theta=0°$) to pronounced coupling ($\Theta=30°$ and 45°). We also plot the electron displacement $\langle x(t)\rangle$ resulting from the current. This plot is appropriate for discussing experimental results obtained by electro-optic detection since the signals in this case are due to internal electric fields generated by the displaced charges.[30] The plot also allows an easy separation of the two contributions to the resonant self-induced current, (i) that of the stationary drift current[31] (represented by the steepness

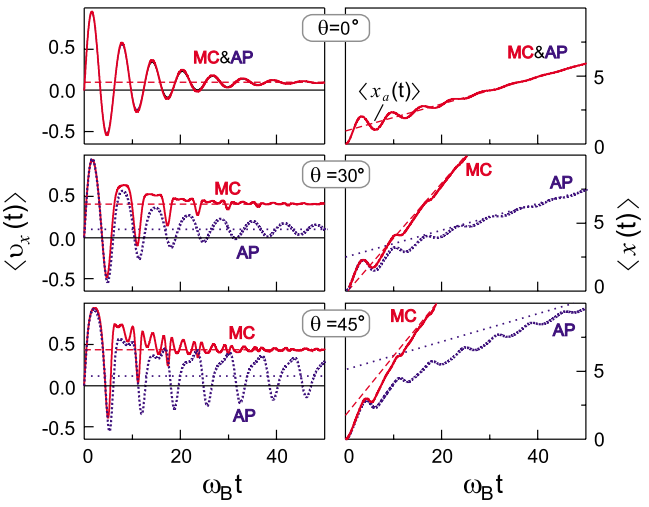

FIG. 3. (Color online) Left panels: Transients of velocity $\langle v_x(t)\rangle$ for $\omega_{cx}=\omega_B$ calculated with the average-particle model (AP) and the simple Monte Carlo model (MC) for three tilt angles Θ of the magnetic field. Right panels: Displacement $\langle x(t)\rangle$ obtained by integration of $\langle v_x(t)\rangle$ over dimensionless time $\omega_B t$. Unit of displacement is V_{max}/ω_B. Thin straight lines mark the asymptotic behavior of these quantities. Relaxation rate $\Gamma=\Gamma_{in}=0.1\omega_B$, $\Gamma_{el}=0$, and effective-mass ratio $A=0.6$.

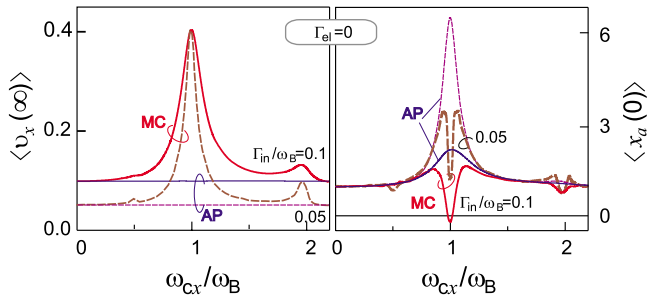

FIG. 4. (Color online) Stationary velocity $\langle v_x(\infty)\rangle$ (left panel) and displacement $\langle x_a(0)\rangle$ (right panel) calculated with the average-particle model (AP, thin lines) and the simple Monte Carlo model (MC, thick lines) for $\Theta=30°$ as a function of ω_{cx}. Relaxation rates $\Gamma=\Gamma_{in}=0.05\omega_B$ and $0.1\omega_B$, $\Gamma_{el}=0$, and effective-mass ratio $A=0.6$.

$\langle v_x(\infty)\rangle$ of the asymptotic line $\langle x_a(t)\rangle$) and (ii) that of the transient current[30] (represented in integrated form by the offset $\langle x_a(0)\rangle$ of the asymptotic line).

For zero coupling, the AP and the MC methods give identical results for the BO oscillation (the CO remains at rest), showing that both models adequately describe the damping of the isolated BO. Large discrepancies between the models, however, arise for the coupled system at resonance. For the parameters chosen, which are close to experimentally relevant values,[30,31] the stationary currents differ by nearly an order of magnitude, and the displacements due to the transients are correspondingly different. The BO oscillations in the AP model show a clear tendency to become self-sustained (dedamped) for increased coupling. This is a remarkable effect since the oscillations of both oscillators die away in the uncoupled state. The dedamping can be understood as a result of positive feedback within the BO-CO loop in connection with Bloch gain of the BO. Full dedamping corresponding to unstability and ending in limit cycles or chaos is reached at stronger coupling and will be discussed below. In the MC model, however, the oscillations are at least as strongly damped as in the uncoupled case, and no tendency to maintained oscillations is seen.

Figure 4 shows the resonances of the drift current and of the asymptotic displacement $\langle x_a(0)\rangle$ due to the integrated transient current, plotted as a function of ω_{cx} for fixed ω_B. The line shapes of the resonances again are drastically different for the two models. In particular, the stationary current is practically independent of ω_{cx} in the AP model whereas it shows a sharply resonant enhancement in the MC model giving rise to peaks at the Bloch frequency and its harmonics and subharmonics. On the other hand, the asymptotic displacement by the transient current exhibits peaks in the AP model which in the MC model turn into dips whose depth changes with damping. As already mentioned above, the MC simulations of $\langle v_x(\infty)\rangle$ with reset to zero should give the same results as those obtained by application of the kinetic formula which was also used in Ref. 31. We indeed found good agreement (data not shown). Furthermore, the peaks and dips in Fig. 4 which appear in the MC model can also be qualitatively reproduced using the AP-type three-dimensional (3D) model of Ref. 33 with damped cyclotron motion. However, since here the current permanently oscil-

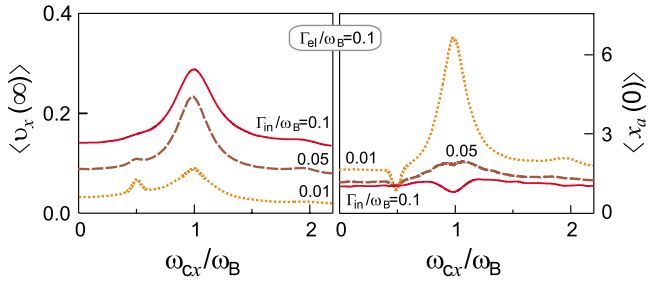

FIG. 5. (Color online) Same quantities as in Fig. 3 calculated as a function of ω_{cx} with the Monte Carlo model for $\Theta=30°$ taking into account elastic scattering ($\Gamma_{el}=0.1\omega_B$) and inelastic scattering ($\Gamma_{in}=0.01\omega_B$, $0.05\omega_B$, and $0.1\omega_B$). Effective mass ratio $A=0.6$.

lates, one has to regard the time average of the current. A serious discrepancy arises for the background drift current where both the MC and the 4D AP model show a constant Esaki-Tsu current contribution. In the damped 3D model of Ref. 33, the dc goes to zero with decreasing cyclotron frequency, due to the neglect of direct damping of the Bloch oscillations by inelastic scattering.

For further exploration, we additionally include elastic scattering in the MC model. As stated above, we regard transitions which lead from a given initial $\vec{k}$ state to a stochastically chosen final state in the Brillouin zone under energy conservation. Figure 5 displays results analogous to those of Fig. 4 for fixed Γ_{el} and decreasing Γ_{in}. With lower Γ_{in} and, hence, increasing influence of Γ_{el}, the stationary velocity curves and the shapes of the displacement resonances become more similar to the curves obtained in the AP model. The stationary current becomes weaker but does not lose its resonance structure whereas the displacement dip turns into a peak again.

We now turn to parameter regions where the transients with start from zero in the AP-model approach limit cycles or chaotic solutions. We confine the consideration to inelastic scattering and disregard a detailed analysis of the routes to chaos and the intricate structures of chaotic attractors. Such an analysis has been comprehensively done in Ref. 33 for the AP-type model used there, which operates in 3D phase space. Similarly complex phenomena are also expected in our AP model in 4D phase space. However, the question arises, whether important characteristics of chaotic dynamics will persist in the framework of the MC approach.

As a gross guideline for exploration of parameter space we perform a linear stability analysis of the constant-current solutions treated above. These solutions follow from Eqs. (4)–(7) by setting the time derivatives to zero and solving for $\langle v_x\rangle=\langle v_x(\infty)\rangle$ (here shortly written as $\langle v_x^\infty\rangle$). One obtains a cubic equation

$$a^2\langle v_x^\infty\rangle^3 - 2a\omega_B\langle v_x^\infty\rangle^2 + (\omega_B^2+\Gamma a+\Gamma^2)\langle v_x^\infty\rangle - \Gamma\omega_B = 0,$$

where $a=\Gamma\omega_{cz}^2/(\omega_{cx}^2+\Gamma^2)$. From $\langle v_x^\infty\rangle$, the remaining quantities are obtained as $\langle v_y^\infty\rangle=-a\langle v_x^\infty\rangle/\omega_{cz}\sqrt{A}$, $\langle v_z^\infty\rangle=-\omega_{cx}\langle v_y^\infty\rangle/\Gamma$, and $\langle\epsilon_x^\infty\rangle=1-\Gamma\langle v_x^\infty\rangle/\Omega_B$ with the shifted $\Omega_B=\omega_B+\omega_{cz}\sqrt{A}\langle v_y^\infty\rangle$. The cubic equation normally has one real solution. More than one real solutions are found for tilt angles close to 90°. We then choose the solution with the lowest

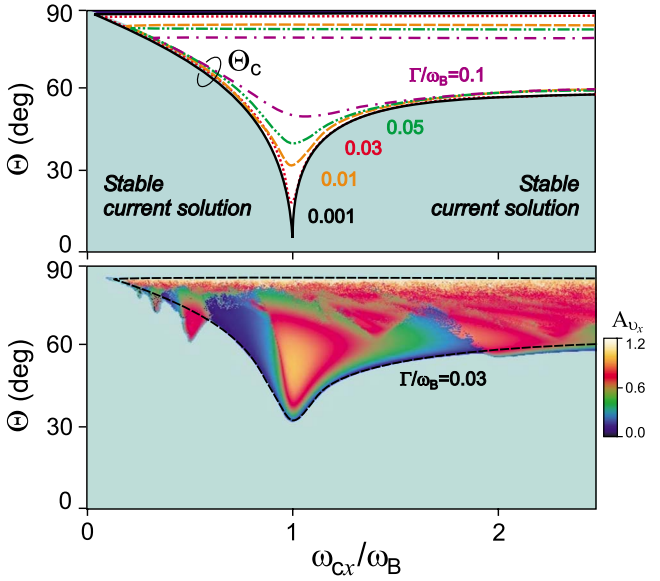

FIG. 6. (Color online) Upper panel: Critical tilt angles Θ_c for stability of the constant-current solutions of Eqs. (4)–(7) for the AP model as a function of CO frequency ω_{cx}/ω_B for different damping frequencies Γ/ω_B. Effective-mass ratio $A=0.6$. The shaded area indicates the tilt angle corresponding to a stable current solution for $\Gamma=0.001\omega_B$. Lower panel: Map of oscillation amplitudes A_{v_x} (peak-to-peak values of $\langle v_x\rangle$) of attractors approached with start from rest. The homogeneously colored background corresponds to $A_{v_x}=0$.

energy. Note, however, that for finite ω_{cx} these tilt angles are not practicable since then $\omega_{cz}\gg\omega_{cx}$ and the magnetic field has to be correspondingly large.

The stability of the constant-current state against small perturbations is tested by linearizing the system around the working point defined by these solutions and by calculating the eigenvalues of the stability matrix $M_{i,j}=\partial F_i/\partial X_j$, where the functions $\vec{F}(\vec{X})$ denote the right sides of Eqs. (4)–(7) in terms of the variables $\vec{X}=(\langle v_x\rangle,\langle\epsilon_x\rangle,\langle v_y\rangle,\langle v_z\rangle)$. The stability limits are marked by vanishing real parts of the eigenvalues of $\hat{M}$, corresponding to just undamped eigenmodes of the coupled oscillators at the working point. For positive real parts, the eigenmodes become dedamped and finally self-sustained, where the amplitudes are limited by the nonlinearities of the system.

Figure 6 shows the critical angle Θ_c for which the constant-current solutions of the AP model become unstable, plotted as a function of ω_{cx}/ω_B for various damping frequencies Γ/ω_B. The critical angle shows a pronounced dip at the fundamental resonance $\omega_{cx}/\omega_B=1$, and narrows and goes to zero for zero damping. It should be noted that the constant solutions can become unstable also if the perturbation at the working point is strong enough to kick the system into a highly nonlinear region. This can happen if the initial condition for the transient grossly deviates from the working point. An example is shown in the lower panel of Fig. 6 which presents peak-to-peak amplitudes of $\langle v_x\rangle$ for oscillating attractors, approached when the particle is started from rest if $\Gamma=0.03\omega_B$. It is seen that near resonances oscillating and constant-current solutions can coexist.

Figure 7 shows $\langle v_x(t)\rangle$ (left panels) and a Lissajous plot of $\langle v_y(t)\rangle$ versus $\langle v_x(t)\rangle$ (right panels), calculated with the AP

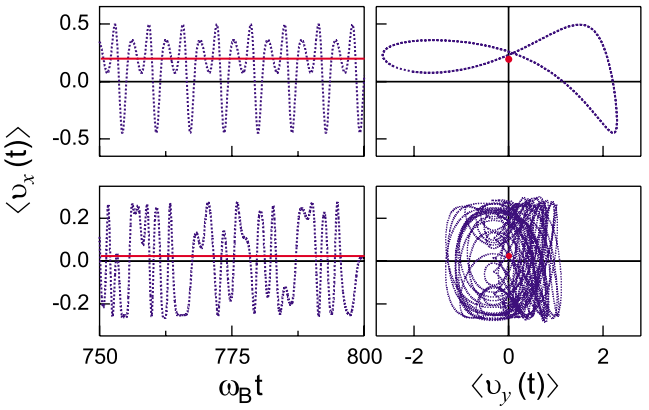

FIG. 7. (Color online) Left panels: Velocity $\langle v_x(t)\rangle$ calculated with the AP model (oscillating curves) and the simple MC model (straight lines), displayed in a time interval long after start of the particles at zero. Right panels: Lissajous plot of $\langle v_y(t)\rangle$ versus $\langle v_x(t)\rangle$. The result of the MC model is a fixed point near the center of the curves. Upper panels: Limit-cycle behavior in the AP model for $\Theta=45°$, $\omega_{cx}=\omega_B$, $\Gamma_{in}=\Gamma=0.03\omega_B$, and $A=0.6$. Lower panels: Chaos in the AP model for $\Theta=60°$, $\omega_{cx}=1.5\omega_B$, $\Gamma_{in}=\Gamma=0.01\omega_B$, and $A=1.2$.

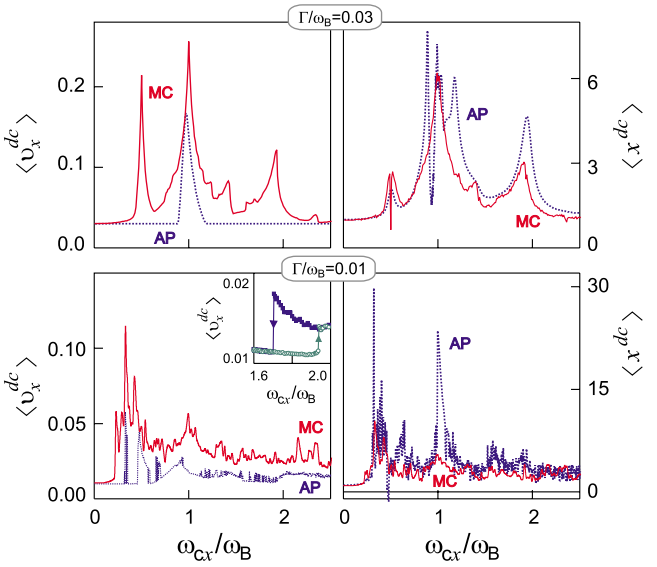

FIG. 8. (Color online) Time average $\langle v_x^{\rm dc}\rangle$ (left panels) and integrated transient current $\langle x^{\rm dc}\rangle$ (right panels) calculated with the AP model (lower curves) and the simple MC model (upper curves) with start from zero. Upper panels and lower panels refer to the same parameters Θ, Γ, and A as in Fig. 7. Insets show hysteresis effects in the AP model using a flying start on upward and downward change in ω_{cx}.

and MC models for different values of tilt angle, cyclotron frequency, damping, and mass ratio. In each case the chosen tilt angle exceeds the critical tilt angle and the transient of the response with start from zero ends either in limit cycles (upper panels) or irregular motion (lower panels). The velocities are plotted within a time interval sufficiently placed behind the transient.

As in the stable region, there are again large discrepancies between the results of the AP and the MC approaches. Most strikingly, the limit-cycle (self-sustained) oscillations and the chaotic movement arising in the AP model are effectively destroyed in the MC model. This directly follows from the MC-based kinetic formula, Eq. (8), where the ac velocity components are suppressed for $t\to\infty$, leaving only the underlying dc contributions (displayed as straight lines, respectively, fixed points in the diagrams of Fig. 7).

Figure 8 shows the time average $\langle v_x^{\rm dc}\rangle$ of the velocity along the SL axis (left panels) performed over the time interval, and the displacement offset $\langle x^{\rm dc}\rangle$ due to the transient (right panels). The displacement offset is obtained by integration of the difference $\langle v_x(t)\rangle - \langle v_x^{\rm dc}\rangle$ over dimensionless time $\omega_B t$ during the transient. The quantities $\langle v_x^{\rm dc}\rangle$ and $\langle x^{\rm dc}\rangle$ are equivalent to $\langle v_x(\infty)\rangle$ and $\langle x_a(0)\rangle$ plotted earlier.

In contrast to the weak-coupling cases at low tilt angles, where the stationary self-induced dc vanishes in the AP model (see Fig. 4), the increase in coupling strength by increasing the tilt angle or the mass ratio now leads to marked contributions to the time-averaged current. For medium coupling (upper panels of Fig. 8), the induced current is confined to an ω_{cx} range where the chosen tilt angle exceeds the critical angle for self-sustained oscillations (see Fig. 6). Further increased coupling (lower panels of Fig. 8) broadens this range, giving rise to detailed structures in the current spectrum which resemble those obtained with the MC model.

The generation of an underlying dc behind the transient in the AP model is due to self-rectification of the self-sustained limit-cycle oscillations or of the chaotic motion of the average particle. The mechanism of down conversion via frequency modulation works only for ac motion. For weak coupling, this kind of motion is absent behind the transient and no resonance peaks are seen in the stationary current. In the MC model, on the other hand, there is always ac motion of individual particles in the ensemble, giving rise to resonant dc.

In small sections of the AP curves one can also see hysteresis effects, like those found in the current spectra of the AP-type model treated in Ref. 33 and attributed to coexistence of distinct attractors belonging to different initial conditions. Hysteresis is observed as an ambiguity of the dc for opposite directions of field variation when using a flying start (instead of a restart from zero) of the particle upon a change in the magnetic field. The inset of Fig. 8 shows results for the AP structures in magnified small intervals of the ω_{cx} scale. The MC results do not show hysteresis throughout. We note that comparison of $\langle v_x^{\rm dc}\rangle$ calculated for strong coupling using either the MC model or the kinetic formula[31] again reveals that both approaches give quantitatively very close results.

The discrepancies between the results of the AP and MC models and the differences in the influence of the scattering processes can be traced back to the approximations made in the AP model. Although the model works well in many situations (beginning with the classical Drude model, characterized by linear dynamics but even for the uncoupled BO and the treatment of Bloch gain[13,15]), the simplifications involved render the AP model problematic for a realistic description of systems with a nonlinear coupling between Bloch and cyclotron oscillations. Two main critical assumptions and approximations of the AP model can be named. One is the substitution (factorization) of ensemble averages over products of

single-particle variables by products of the corresponding AP variables. The other is the introduction of smooth, continuously acting friction terms in the equations of motion instead of stochastic and sudden scattering events.

Regarding factorization, let us discuss as an example the ensemble average $\langle v_x(t)v_y(t)\rangle$ which describes the time-dependent correlation between the velocity components within a particle and which is mainly responsible for the additionally induced current in the constant-current state. This can be seen from Eq. (5) by resubstituting $\langle v_x v_y\rangle$ for $\langle v_x\rangle\langle v_y\rangle$. In the constant-current state one has $\langle \dot{\epsilon}_x\rangle = 0$ and the supplied energy is dissipated with a rate $\Gamma_{in}\langle \epsilon_x\rangle$. Furthermore, $\langle \epsilon_x\rangle \approx 1$ for moderate damping. The magnetic-field-dependent current then is approximately given by $\langle v_x\rangle \approx \Gamma_{in}/\omega_B - \omega_{cz}\sqrt{(A)\langle v_x v_y\rangle}/\omega_B$, where the first term represents the current without field. The power drawn from the electric field by the additional current amounts to $-\omega_{zc}\sqrt{A}\langle v_x v_y\rangle$. It is transferred to the in-plane energy $\langle \epsilon_\perp\rangle = \frac{A}{2}(\langle v_y^2\rangle + \langle v_z^2\rangle)$ and dissipated there with rate $\Gamma_{in}\langle \epsilon_\perp\rangle$.

The correlation can be written as $\langle v_x(t)v_y(t)\rangle = \langle v_x(t)\rangle\langle v_x(t)\rangle + \langle \Delta v_x(t)\Delta v_y(t)\rangle$, where the Δ terms are the differences between the single-particle and the AP variables. It is seen that a factorization is only justified if the second term, which involves the deviations of the velocity of a particle from the mean velocity, can be neglected. A factorization is generally allowed at the very beginning of a transient, when the particles still move coherently and the Δ terms vanish. Quite soon, however, the phase coherence between the particles is lost by scattering. The Δ terms then are nonvanishing and they become relevant if there exists a correlation between the fluctuations $\Delta v_x(t)$ and $\Delta v_y(t)$ belonging to the same particle.

Such a correlation between nonvanishing Δ terms is favored for inelastic scattering by the identical conditions of restart after scattering at random times since all velocity components are reset to zero in our MC model. Thus, a factorization is not allowed and the two models should give grossly different results. In contrast, the velocity components are uncorrelated after elastic scattering since this type of scattering brings the particle into a random state within the Brillouin zone, thus effectively destroying any existing correlation between velocity components. One then expects the results of both models to be closer to each other.

These features are demonstrated in Fig. 9 which shows a plot of $\langle v_x(t)v_y(t)\rangle$ at resonance for two extreme cases with dominant inelastic, respectively, elastic scatterings. The correlation functions are compared to the product of the mean velocities obtained with the AP model for a relaxation rate of the same magnitude. The MC model is mapped to an extended AP model by including relaxation terms in Eqs. (4)–(7) in the following way: $\Gamma_{\epsilon_x} = \Gamma_{in}$, $\Gamma_{v_i} = \Gamma_{in} + \Gamma_{el}$, and $i = x, y, z$.

It can be seen that the (negative) correlation after the transient in the MC model is strongest for dominating inelastic scattering, becomes weaker for dominating elastic scattering but remains slightly different from the AP values (the latter are very small because $\langle v_x(t)\rangle$ and $\langle v_y(t)\rangle$ vanish in the constant-current state for vanishing Γ_{in}). However, the tendency of the correlations of the MC model for elastic scattering to come closer to those of the AP model explains why the behavior of the system in this case resembles qualitatively the results of the AP model (see Fig. 5). The relaxation of $\langle v_x(t)v_y(t)\rangle$ depends on the coupling strength and the scattering rates and is not further investigated here. In contrast to the presented correlation functions which converge to a constant value, the 3D AP-type model of Ref. 33 yields a time-dependent correlation $\langle v_x(t)\rangle\langle v_y(t)\rangle$ with nondecaying oscillations due to the permanent oscillations of the particles.

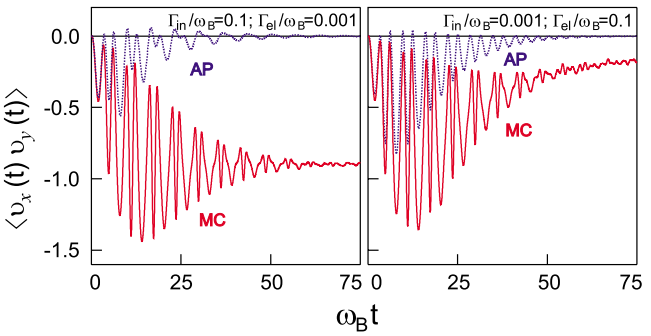

FIG. 9. (Color online) Time-dependent correlation $\langle v_x(t)v_y(t)\rangle$ of the velocity components of a particle in the MC model for dominating inelastic (left panel) and elastic (right panel) scatterings compared with products of velocities obtained in the extended AP model (see text). Parameters: Resonance situation ($\omega_{cx} = \omega_B$), tilt angle $\Theta = 30°$, and effective-mass ratio $A = 0.6$. For dominant inelastic scattering: $\Gamma_{in} = 0.1\omega_B$ and $\Gamma_{el} = 0.001\omega_B$, for dominant elastic scattering: $\Gamma_{in} = 0.001\omega_B$ and $\Gamma_{el} = 0.1\omega_B$.

The second critical assumption of the AP model is the representation of scattering by deterministic, phenomenological relaxation terms in the equations of motion. As seen above, this approximation leads to some interesting phenomena of particle motion which do not appear in the MC description.

First of all, the AP model predicts sustained oscillatory motion of the ensemble such as dedamped transient oscillations and limit cycles. As already mentioned, such oscillations without external ac driving fields are possible because of Bloch gain and positive feedback in the BO-CO loop. After some kind of synchronization (e.g., by particle-particle interaction or by weak external ac fields) to overcome field inhomogeneities and slightly different initial conditions, the oscillations might show up in the macroscopic currents as possible sources of terahertz radiation. In the MC model, on the contrary, the stochastic forces in the long-time limit severely modify the phase relations between the motion of different particles. These perturbations therefore result in destructive interference of all ac contributions to the ensemble average after the transient.

A similar argument should also apply to hysteresis effects in the dc characteristics of the coupled motion, which one expects to see in experiments as a clear signature of multistability effects in chaotic dynamics.[33] Hysteresis is connected with a memory of the preceding trajectory a particle experiences before the external fields are changed. This memory is easily destroyed by the stochastic forces which lie at the heart of the MC model. Moreover, the question arises as to what kind of structures will remain as a compromise

between Hamiltonian chaos due to the free motion and dissipative chaos due to damping. It is expected that only a few fundamental and robust signatures like that based on the resonance conditions will survive.

IV. FULL-SCALE MONTE CARLO SIMULATIONS

In view of the sensitive dependence of the resonance curves of the induced dc on the scattering mechanisms (see Figs. 4 and 5) and on the values of the model parameters (see Figs. 7 and 8), we consider in the following the scattering mechanisms in more detail, taking into account realistic selection rules, and also choose parameters matched more closely to presently achievable experimental conditions. We perform MC simulations of the particle ensemble in a superlattice subject to both electric and magnetic fields using the synchronous-ensemble method.[44] We consider electron motion within the miniband transport approach.[35] This ansatz imposes restrictions on the superlattice miniband width Δ which for an applied electric field F_x has to obey the condition $eF_xd<\Delta$, where d is the spatial period of the superlattice. The field needed to observe Bloch oscillations under realistic conditions is typically not less than 10 kV/cm.[8–12] Only then is the Bloch frequency larger than the scattering rate at low temperatures. The miniband width, according to $eF_xd<\Delta$, should be larger than 30 meV for typical values of d in order to ensure that the simulations remain within the validity range of the miniband transport approach. Similar conditions have to be imposed to the cyclotron frequencies.

We consider two GaAs/$Al_{0.3}Ga_{0.7}As$ superlattices which have the same spatial period ($d=8.48$ nm) but differ in their miniband width due to the different quantum-well (GaAs layer) and barrier ($Al_{0.3}Ga_{0.7}As$ layer) thicknesses. Δ is calculated by means of the Kronig-Penney model[45] and amounts to 33 and 69 meV, respectively.

We treat inelastic electron scattering with optical phonons via Froehlich interaction, and with acoustic phonons via deformation-potential coupling. The expressions for the scattering rates are represented in Ref. 19. All material parameters, necessary for the calculation of the scattering rates, are chosen to be the same as for bulk GaAs, namely, the effective electron mass $0.067m_0$, where m_0 is the free-electron mass, the static and high-frequency dielectric constants 12.9 and 10.9, respectively, the optic-phonon energy 36.2 meV, the acoustic deformation potential 7 eV, and the density 5.37 g/cm^3.

Elastic scattering is included via interface-roughness scattering of the electrons. It is described by a δ-function-type scattering potential energy $U(x,r)=\xi(r)\Delta E_c\delta(x-x_0)$ for an interface located at $x=x_0$ and exhibiting spatial fluctuations on the order of $\pm\eta$ described by a random function $\xi(r)$.[46] We use $\eta=0.28$ nm which corresponds to the thickness of one monolayer of GaAs. The conduction-band discontinuity ΔE_c between GaAs and $Al_{0.3}Ga_{0.7}As$ is 0.243 eV. We assume a Gaussian form of the surface-roughness correlation function $\langle\xi(r)\xi(r')\rangle$ in the direction parallel to the surface with a correlation length λ of 3 nm. The simulations are performed for a lattice temperature T of 10 K assuming an initial electron distribution over the Brillouin zone according to a Gaussian function $P(k_x,k_y,k_z)\propto\exp\{-\hbar^2(Ak_x^2+k_y^2+k_z^2)/(2m_{yy}k_BT)\}$, where k_B is the Boltzmann constant.

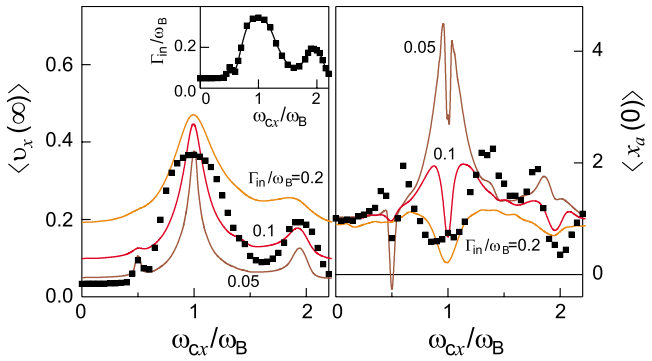

FIG. 10. (Color online) Stationary velocity $\langle v_x(\infty)\rangle$ (left panel) and asymptotic displacement $\langle x_a(0)\rangle$ (right panel) of the $\langle v_x(t)\rangle$ transient as a function of ω_{cx}. Data calculated for a superlattice with a miniband width of 33 meV using the simple (lines) and advanced (symbols) MC models for $\Theta=30°$. Elastic scattering is neglected and the inelastic-scattering rates for the simple MC model are $\Gamma_{in}=0.05\omega_B$, $0.1\omega_B$, and $0.2\omega_B$; the Bloch frequency for the advanced MC model is $\omega_B/2\pi=1.9$ THz. Inset: Relative inelastic-scattering rate versus ω_{cx} calculated with the advanced MC model.

The relevant difference between the more advanced MC model and the simplified version employed earlier in the paper is that the rate of inelastic scattering is not constant and depends on the magnetic field. Inelastic scattering can only occur if the kinetic energy of an electron is larger than the respective phonon energy. Considering that scattering via optical phonons dominates the total inelastic rate, the miniband width has a strong influence on the scattering rate. For a superlattice with a miniband width smaller than the optical-phonon energy (36.2 meV), scattering with optical-phonon emission is eliminated at low temperature if no magnetic field is applied. This changes with magnetic field because the field couples the motion of the electrons in the miniband to the in-plane motion. This gives rise to an increase in the total particle energy and thus opens an additional channel for electron scattering with optical-phonon emission. The inset of Fig. 10 illustrates the magnetic-field dependence of the inelastic-scattering rate Γ_{in} for the superlattice with $\Delta=33$ meV. The scattering rate increases with increasing magnetic field and peaks at resonances of the cyclotron frequency with the Bloch frequency, reaching a maximal value of $0.35\omega_B$.

The main panel of Fig. 10 shows stationary velocity and displacement curves for different inelastic-scattering rates obtained with both the simple and the advanced MC models. The results are very similar. The central physical features are captured even if a simplified description of the scattering processes is employed. Interestingly, the advanced MC simulations also reproduce the dips in the asymptotic displacement $\langle x_a(0)\rangle$ found at $\omega_{cx}/\omega_B=0.5,1,2$ with the simple model (see also Figs. 4 and 5). Furthermore, no sustained oscillations and no hysteresis are observed. The dips originate from the inelastic scattering which repeatedly brings a particle close to the bottom of the miniband thus resulting in a motion which resembles the motion from rest treated in the simple model.

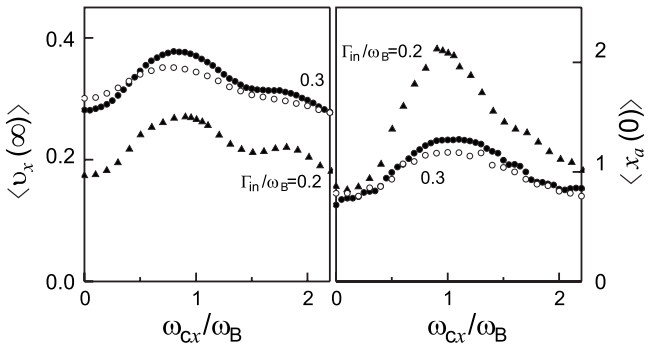

FIG. 11. Same quantities as in Fig. 10 for the superlattice with a miniband width of 69 meV. All simulations performed by the advanced MC model neglecting elastic interface-roughness scattering (full symbols) and including it (open symbols) with correlation length $\lambda=3$ nm. Parameters: Bloch frequency $\omega_B/2\pi=1.9$ THz (circles) and 3.1 THz (triangles); average relative inelastic-scattering rates $\Gamma_{in}=0.3\omega_B$ and $0.2\omega_B$.

Inclusion of elastic interface-roughness scattering in the MC model does not change the shape of the displacement curve dramatically (data not shown). The elastic scattering makes the motion of a particle more stochastic which is reflected in a flatter displacement curve. It still shows a shallow dip at $\omega_{cx}/\omega_B=1$ for a certain range of correlation lengths of the interface-roughness scattering while the dips at $\omega_{cx}/\omega_B=0.5$ and 2 are smeared out.

The picture changes drastically if we focus on the particle dynamics in a superlattice with a miniband width larger than the optical-phonon energy. Note, that a larger miniband width entails a stronger randomization of the final particle states after scattering with phonon emission. The electron is transferred not only to positions close to $\vec{k}=\vec{0}$, but, as in the case of elastic scattering, also to other states within the Brillouin zone which are now allowed by energy conservation. Moreover, since a particle has enough energy to experience scattering with optical-phonon emission even at low temperature, the magnetic field does not affect the inelastic-scattering rate as much as for a superlattice with a smaller miniband width. Thus, the relative inelastic-scattering rate remains approximately the same over the whole cyclotron frequency range considered here, and is only changed by the chosen Bloch frequency.

Figure 11 displays the stationary velocity and asymptotic displacement curves for the superlattice with $\Delta=69$ meV. Both types of curves show a peak at or close to $\omega_{cx}/\omega_B=1$ which for the displacement curve becomes better pronounced with a decrease in the relative inelastic-scattering rate, i.e., an increase in the Bloch frequency. Interface-roughness scattering smears out the peak slightly due to the additional randomization of the particle motion.

The temperature affects both the initial distribution of the electrons in the miniband as well as the scattering rates. As the lattice temperature increases, the scattering with optical-phonon absorption becomes possible and leads to a stronger randomization of the final particle states after scattering. The particle dynamics in a superlattice at room temperature is to a certain extent similar to that of a superlattice at low temperature but with a miniband width larger than the optical-phonon energy. The calculations for the superlattice with a miniband width of 33 meV and lattice temperature of 300 K show that the stationary velocity and the displacement curves demonstrate a peak close to $\omega_{cx}/\omega_B=1$ while the peak at $\omega_{cx}/\omega_B=2$ is completely washed out (data not shown). The height of the peak decreases by a factor of 2.5 with temperature increase from 10 to 300 K.

We note, that our simple MC model, for dominant elastic-scattering predicts correctly the peak of the particle displacement which has been observed experimentally for a superlattice in a tilted magnetic field and a miniband width smaller than the optical-phonon energy.

V. CONCLUSIONS

In conclusion, we showed within the miniband transport approach that average-particle models and Monte Carlo simulations make quite different predictions with respect to the time dependence of the velocities of an electron ensemble in a superlattice subjected to an electric field and a tilted magnetic field. The average-particle model used by us operates in a 4D phase space and in contrast to a 3D model used earlier in the literature,[33] allows to treat direct damping of all three velocity components of the particles. We mainly study the currents along the electric field, both the integrated dc during the transient after optical-pulse excitation and the drift current in the long-time limit. These currents are due to down conversion of the coupled oscillatory motion of the Bloch and cyclotron oscillators and show marked resonances. The deviations in the results of the 4D and 3D average-particle and the Monte Carlo treatment are already revealed in the weak-coupling limit and for dominant inelastic scattering, where either widely different shapes of resonance curves (4D model) or different magnitudes of background currents (3D model) and of the relaxation rates are observed. However, the results of the 4D average-particle and the Monte Carlo models for the resonance curves of the currents come close to each other if elastic scattering dominates over the inelastic one.

The discrepancies are a result of the approximations of the average-particle model, in which ensemble averages over products of particle variables are factorized into products of the average variables, and scattering events are represented by continuous relaxation terms in the equations of motion. Most importantly, the simplifications lead to some artifacts for stronger coupling strength and in the long-time limit, notably self-sustained regular oscillatory motion and hysteresis in the dc characteristics. Both effects are easily destroyed by the abrupt scattering events on which the Monte Carlo approach is based. Having in mind possible terahertz applications, the prediction of dedamped and self-sustained oscillations therefore wrongfully suggests the possibility to enhance and prolong terahertz radiation of electron bunches after optical-pulse excitation, during their dwell time in the superlattice, i.e., the possibility to realize practical sources of terahertz radiation.

ACKNOWLEDGMENTS

N.V.D. thanks the Physikalisches Institut of the Johann Wolfgang Goethe-Universität for hospitality. This work was partially supported by Grant No. BF5M01 of the Russian Ministry of Education and the U.S. Civilian Research and Development Foundation.

[1] C. Zener, Proc. R. Soc. London, Ser. A **145**, 523 (1934).
[2] L. Esaki and R. Tsu, IBM J. Res. Dev. **40**, 61 (1970).
[3] A. Sibille, J. F. Palmier, H. Wang, and F. Mollot, Phys. Rev. Lett. **64**, 52 (1990).
[4] A. Wacker, A.-P. Jauho, S. Rott, A. Markus, P. Binder, and G. H. Dohler, Phys. Rev. Lett. **83**, 836 (1999).
[5] E. Schomburg, T. Blomeier, K. Hofbeck, J. Grenzer, S. Brandl, I. Lingott, A. A. Ignatov, K. F. Renk, D. G. Pavel'ev, Yu. Koschurinov, B. Ya. Melzer, V. M. Ustinov, S. V. Ivanov, A. Zhukov, and P. S. Kop'ev, Phys. Rev. B **58**, 4035 (1998).
[6] S. Rott, N. Linder, and G. H. Doehler, Phys. Rev. B **65**, 195301 (2002).
[7] Yu. A. Tarakanov, V. Vettchinkina, M. A. Odnoblyudov, K. A. Chao, N. Sekine, and K. Hirakawa, Phys. Rev. B **72**, 125345 (2005).
[8] J. Feldmann, K. Leo, J. Shah, D. A. B. Miller, J. E. Cunningham, T. Meier, G. von Plessen, A. Schulze, P. Thomas, and S. Schmitt-Rink, Phys. Rev. B **46**, 7252 (1992).
[9] K. Leo, P. H. Bolivar, F. Brueggemann, R. Schwedler, and K. Koehler, Solid State Commun. **84**, 943 (1992).
[10] C. Waschke, H. G. Roskos, R. Schwedler, K. Leo, H. Kurz, and K. Kohler, Phys. Rev. Lett. **70**, 3319 (1993).
[11] R. Martini, G. Klose, H. G. Roskos, H. Kurz, H. T. Grahn, and R. Hey, Phys. Rev. B **54**, R14325 (1996).
[12] T. Dekorsy, P. Leisching, K. Kohler, and H. Kurz, Phys. Rev. B **50**, 8106 (1994).
[13] S. A. Ktitorov, G. S. Simin, and V. Y. Sindalovskii, Sov. Phys. Solid State **13**, 1872 (1972).
[14] P. J. Price, IBM J. Res. Dev. **17**, 39 (1973).
[15] A. A. Ignatov, K. F. Renk, and E. P. Dodin, Phys. Rev. Lett. **70**, 1996 (1993).
[16] H. Kroemer, arXiv:cond-mat/0007482 (unpublished).
[17] H. Willenberg, G. H. Doehler, and J. Faist, Phys. Rev. B **67**, 085315 (2003).
[18] E. Schomburg, N. V. Demarina, and K. F. Renk, Phys. Rev. B **67**, 155302 (2003).
[19] N. V. Demarina and K. F. Renk, Phys. Rev. B **71**, 035341 (2005).
[20] A. Lisauskas, M. M. Dignam, N. V. Demarina, E. Mohler, and H. G. Roskos, Appl. Phys. Lett. **93**, 021122 (2008).
[21] T. Hyart, K. N. Alekseev, and E. V. Thuneberg, Phys. Rev. B **77**, 165330 (2008).
[22] K. Unterrainer, B. J. Keay, M. C. Wanke, S. J. Allen, D. Leonard, G. Medeiros-Ribeiro, U. Bhattacharya, and M. J. W. Rodwell, Phys. Rev. Lett. **76**, 2973 (1996).
[23] P. D. Savvidis, B. Kolasa, G. Lee, and S. J. Allen, Phys. Rev. Lett. **92**, 196802 (2004).
[24] R. Terazzi, T. Gresch, M. Giovannini, N. Hoyler, N. Sekine, and J. Faist, Nat. Phys. **3**, 329 (2007).
[25] S. Winnerl, E. Schomburg, S. Brandl, O. Kus, K. F. Renk, M. C. Wanke, S. J. Allen, A. A. Ignatov, V. Ustinov, A. Zhukov, and P. S. Kop'ev, Appl. Phys. Lett. **77**, 1259 (2000).
[26] K. F. Renk, B. I. Stahl, A. Rogl, T. Janzen, D. G. Pavel'ev, Yu. I. Koshurinov, V. Ustinov, and A. Zhukov, Phys. Rev. Lett. **95**, 126801 (2005).
[27] K. N. Alekseev, M. V. Gorkunov, N. V. Demarina, T. Hyart, N. V. Alexeeva, and A. V. Shorokhov, Europhys. Lett. **73**, 934 (2006).
[28] T. Hyart, A. V. Shorokhov, and K. N. Alekseev, Phys. Rev. Lett. **98**, 220404 (2007).
[29] F. G. Bass, V. V. Zorchenko, and V. I. Shashora, JETP Lett. **31**, 314 (1980).
[30] Yu. A. Kosevich, A. B. Hummel, H. G. Roskos, and K. Köhler, Phys. Rev. Lett. **96**, 137403 (2006); Phys. Status Solidi B **243**, 2405 (2006).
[31] T. M. Fromhold, A. A. Krokhin, C. R. Tench, S. Bujkiewicz, P. B. Wilkinson, F. W. Sheard, and L. Eaves, Phys. Rev. Lett. **87**, 046803 (2001); T. M. Fromhold, A. Patane, S. Bujkiewicz, P. B. Wilkinson, D. Fowler, D. Sherwood, S. P. Stapleton, A. A. Krokhin, L. Eaves, M. Henini, N. S. Sankeshwar, and F. W. Sheard, Nature (London) **428**, 726 (2004).
[32] D. Fowler, D. P. Hardwick, A. Patane, M. T. Greenaway, A. G. Balanov, T. M. Fromhold, L. Eaves, M. Henini, N. Kozlova, J. Freudenberger, and N. Mori, Phys. Rev. B **76**, 245303 (2007).
[33] A. G. Balanov, D. Fowler, A. Patane, L. Eaves, and T. M. Fromhold, Phys. Rev. E **77**, 026209 (2008).
[34] M. Tinkham, *Introduction to Superconductivity* (McGraw-Hill, New York, 1996).
[35] A. Wacker and A.-P. Jauho, Phys. Rev. Lett. **80**, 369 (1998); A. Wacker, Phys. Rep. **357**, 1 (2002).
[36] T. Bauer, J. Kolb, A. B. Hummel, H. G. Roskos, Yu. Kosevich, and K. Kohler, Phys. Rev. Lett. **88**, 086801 (2002).
[37] A. A. Ignatov and V. I. Shashkin, Phys. Lett. A **94**, 169 (1983).
[38] K. N. Alekseev, G. P. Berman, D. K. Campbell, E. H. Cannon, and M. C. Cargo, Phys. Rev. B **54**, 10625 (1996).
[39] E. H. Cannon, F. V. Kusmartsev, K. N. Alekseev, and D. K. Campbell, Phys. Rev. Lett. **85**, 1302 (2000); Y. A. Kosevich, *ibid.* **88**, 229701 (2002) Comment; E. H. Cannon, F. V. Kusmartsev, K. N. Alekseev, and D. K. Campbell, *ibid.* **88**, 229702 (2002) Reply.
[40] A. Patane, A. Ignatov, L. Eaves, P. C. Main, M. Henini, E. Schomburg, R. Scheuerer, K. F. Renk, V. M. Ustinov, A. E. Zhukov, and A. R. Kovsh, Phys. Rev. B **66**, 075325 (2002).
[41] C. Wang and J. C. Cao, Phys. Rev. B **72**, 045339 (2005).
[42] A. Sibille, J. F. Palmier, A. Celeste, J. C. Portal, and F. Mollot, EPL **13**, 279 (1990).
[43] See, for example, J. C. Butcher, *Numerical Methods for Ordinary Differential Equations* (Wiley, New York, 2003).
[44] C. Jacoboni and L. Reggiani, Rev. Mod. Phys. **55**, 645 (1983).
[45] G. Bastard, *Wave Mechanics Applied to Semiconductor Heterostructures* (Les Editions de Physique, Paris, 1988).
[46] G. Etemadi and J. F. Palmier, Solid State Commun. **86**, 739 (1993).